



Dynamic thermal radiation modulators via mechanically tunable surface emissivity

Songshan Zeng^{1,2,†}, Kuangyu Shen^{1,2,†}, Yin Liu³, Aimee P. Chooi², Andrew T. Smith², Shihao Zhai², Zi Chen^{3,*}, Luyi Sun^{1,2,4,*}

¹ Polymer Program, Institute of Materials Science, University of Connecticut, Storrs, CT 06269, USA

² Department of Chemical and Biomolecular Engineering, University of Connecticut, Storrs, CT 06269, USA

³ Thayer School of Engineering, Dartmouth College, Hanover, NH 03755, USA

⁴ Department of Biomedical Engineering, University of Connecticut, Storrs, CT 06269, USA

Inspired by cephalopods, we design a hybrid structure comprised of a rigid film with a low thermal emissivity and a substrate with a high thermal emissivity combined with a stretchable heater. The film's topography is characterized by distributed strain-dependent micro-cracks, enabling the exposure of the substrate to be tuned by the applied strain. Thus, the effective surface thermal emissivity originating from the combination of the film and the exposed substrate can be instantaneously and reversibly modulated simply via mechanical means. The system exhibits various pronounced advantages, including ease of fabrication, low working temperature, broad emissivity modulation range, observing angle independence, excellent reversibility, instantaneous response, high strain sensitivity, feasibility for patterning and multiplexing, and autonomous actuation. Additionally, the system demonstrates intriguing thermographic-based applications in finger motion sensing, information encryption, multiplexing display, and thermal camouflage. Therefore, this work can facilitate the invention of next-generation thermal modulators with autonomous, on-demand, and board-range control.

Introduction

Some biological systems have evolved to tune their skin coloration/reflectivity in an instant, on-demand fashion [1–10]. Recently, similar artificial thermal/infrared (IR) radiation modulators have been developed, which can be leveraged for thermal camouflage [5,11–12], packaging [13], radiative cooling [14–15], thermophotovoltaics [16–17], thermal communication [18–19], thermoregulation [6], and so on. The radiation modulation is realized by engineering the thermal emissivity via various techniques, including thermochromic pigments [20–21], semiconductors [22–23], electrochromic devices [24–25], metastructured

materials [5,26], and phase transition compounds [27–28]. Although decent progress has been achieved, these efforts still face various limitations, such as narrow modulation range [22–23], low response rate [25], complexity of fabrication [5], hysteresis during cycling [20–21], high working temperature [26,29–30], etc. Researchers have since turned to natural systems to seek inspiration for potential solutions [31–37], such as, *Cephalopod*, a marine life with sophisticated skin structures responsible for displaying fascinating color/iridescence changes [1,7,35]. Generally, two types of cells in the dermal layer function in tandem to demonstrate different optical performances. The first type of cells are iridocytes, which present periodical arrangements of protein building blocks and extracellular space [33,35,37], acting as a tunable Bragg stacking geometry for actively controlling the light scattering, refraction, and reflection [33]. The second type of cells

* Corresponding authors.

E-mail addresses: Chen, Z. (zi.chen@dartmouth.edu), Sun, L. (luyi.sun@uconn.edu).

† These authors made equal contribution to this work.

are chromatophores, which contain internal pigment sacculi encircled by radial cells, and the expansion and contraction of radial cells can control the exposure and concealment of underlying pigment to modulate the corresponding color visibility [1–2,9–10]. Most of the current cephalopod-inspired thermal modulators focus on tuning the dynamic wrinkle structures via mechanical strain [32–33,35–37] and patterning [31], which mimic the optical modulation mechanism of iridocytes. These modulators mainly utilize the periodical and rough topographies of wrinkles, which present different infrared/visible light scattering, refraction, and reflection properties to that of the flat surface. However, these designs still have some limitations, such as relatively low strain responsive sensitivity [32,34–37], narrow modulation range, [31–32,35–36] and low angle independence [31]

Herein, to address the aforementioned issues, we propose a new type of cephalopod-inspired system that directly modulates the surface thermal radiation via mechanical strain. Unlike the above modulators, the inspiration of this new design is abstracted from the chromatophores instead of iridocytes. The system is made of a multi-layered structure containing a thermal radiation shielding rigid film with a low thermal emissivity ($\varepsilon = 0.49$) and a soft substrate with a high thermal emissivity ($\varepsilon = 0.98$) equipped with an underlying stretchable heater. Notably, the heater is only used to heat up the device to the preset working temperature so that the system can emit thermal radiation to the external environment. Thus, the heater is not used to modulate the thermal radiation in this system. The film topography is defined by uniformly distributed strain-dependent micro-cracks, which mimic the radial cells on the chromatophores, which can tune the exposure of underlying substrate via the mechanically controllable crack width. Herein, the effective surface thermal emissivity of the device is defined as the combination of the emissivity of the film and the exposed substrate, which is a function of mechanical strain. Since the film and substrate have a striking contrast on the emissivity ($\Delta\varepsilon = 0.49$), the effective emissivity is supposed to be highly sensitive to the strain-dependent exposure area of the substrate. As such, the thermal radiation of this system can be instantaneously and reversibly modulated simply via mechanical means with a large modulation range. This new design also results in angle independent performance, due to the omnidirectional emission of thermal radiation. Two types of hybrid structures were designed for operation under in-plane uniaxial strain and out-of-plane bulging strain, respectively. The system can exhibit various advantages, such as low working temperatures, observing angle independence, high strain sensitivity, instantaneous response, excellent cyclability, feasibility of patterning and multiplexing, etc. The structure also enables potential applications under thermographic vision, including sensing finger motion, information encryption, multiplexing dynamic display, and thermal camouflage.

Results and discussion

Design and performance of the thermal modulating system for uniaxial strain (TMSU)

The emissivity (ε) is defined as the ratio of the thermal radiation emitted from the sample to that emitted from a perfect emitter

(i.e., a blackbody) at the same temperature and wavelength [38]. As shown in Fig. 1(a), the thermal modulating system for uniaxial strain (TMSU) is comprised of a layer of mirror chrome (MC) coating (containing thin aluminum flakes) with a low emissivity ($\varepsilon = 0.49$) atop a polyvinyl alcohol (PVA)/laponite composite transition layer bonded to an Ecoflex® stretchable substrate with a high emissivity ($\varepsilon = 0.98$). A stretchable heater made of serpentine patterned conductive thread sandwiched by 3 M VHB™ stretchable double-sided tape (see Fig. S1 for performance) is attached underneath the substrate, which can maintain the same heating temperature within the operation range. To generate more distributed micro-cracks on the thin film composed of the MC and PVA/laponite layers, a pre-stretching strain of 200% was applied and subsequently released. The opening/closing of the micro-cracks enables the exposure of the substrate with a high emissivity to be regulated by mechanical strain (Fig. 1(a)). Typically, in this work, the modulator is placed in an ambient environment (T_a (ambient temperature) = 24 °C, unless otherwise mentioned) and heated up to 45 °C by the heater (T_s (sample temperature) = 45 °C, unless otherwise mentioned), enabling it to emit thermal radiation to the external environment that can be monitored by a thermal camera or sensor. And this working temperature is lower than those of the thermal modulators based on electrical heating [29,30].

Heat flux is defined as the flow of thermal energy travelling through a given region per unit area per unit time [39], which is mainly in the form of thermal radiation in this work. According to the classical Stefan-Boltzmann law and the proposed geometrical model (see Fig. S2) for cracks, the theoretical heat flux emitted from the heated TMSU to ambient environment is given by (see Methods for detailed information)

$$\bar{q} = \frac{\varepsilon_m + \lambda\varepsilon_e}{1 + \lambda} \sigma (T_s^4 - T_a^4) = \varepsilon_{\text{eff}} \sigma (T_s^4 - T_a^4) \quad (1)$$

where $\sigma = 5.6703 \times 10^{-8} \text{ (W/m}^2\text{K}^4)$ is the Stefan-Boltzmann constant, ε_{eff} is the theoretical effective emissivity given by $\varepsilon_{\text{eff}} = \frac{\varepsilon_m + \lambda\varepsilon_e}{1 + \lambda}$, λ is the total stretching strain, ε_m and ε_e are the experimental emissivity of the MC layer and the Ecoflex® substrate, respectively. As shown in Fig. 1(b), the experimental heat flux emitted from the heated TMSU ($T_s = 45$ °C) was tested by a sensors complex coupled with heat flux and thermocouple temperature measurement (the distance of the sensor to sample surface = 5 mm, size of the tested area = 2.5 cm², all other samples were tested under the same conditions unless otherwise mentioned). The heat flux manifested a progressive growth from 68.7 to 112.6 W/m² as uniaxial strain increased from 0% to 150%, which matches well with the theoretical results. While the temperature for this area, measured by a thermocouple, showed virtually no change and stayed at ca. 28.7 °C.

The strain response of the experimental and theoretical effective emissivity calculated from the heat flux data and the crack width of the TMSU is shown in Fig. 1(c). The experimental emissivity increased from 0.49 at 0% strain to 0.68, 0.77, and 0.81, at 60%, 105%, and 150% strain, respectively, demonstrating an emissivity modulation range up to 0.32 within a 150% strain range. Also, this experimental evolution of emissivity with strain is consistent with the theoretical results. The average crack width on the thin film layers increased to 33.4, 132.9, and 243.5 μm, at

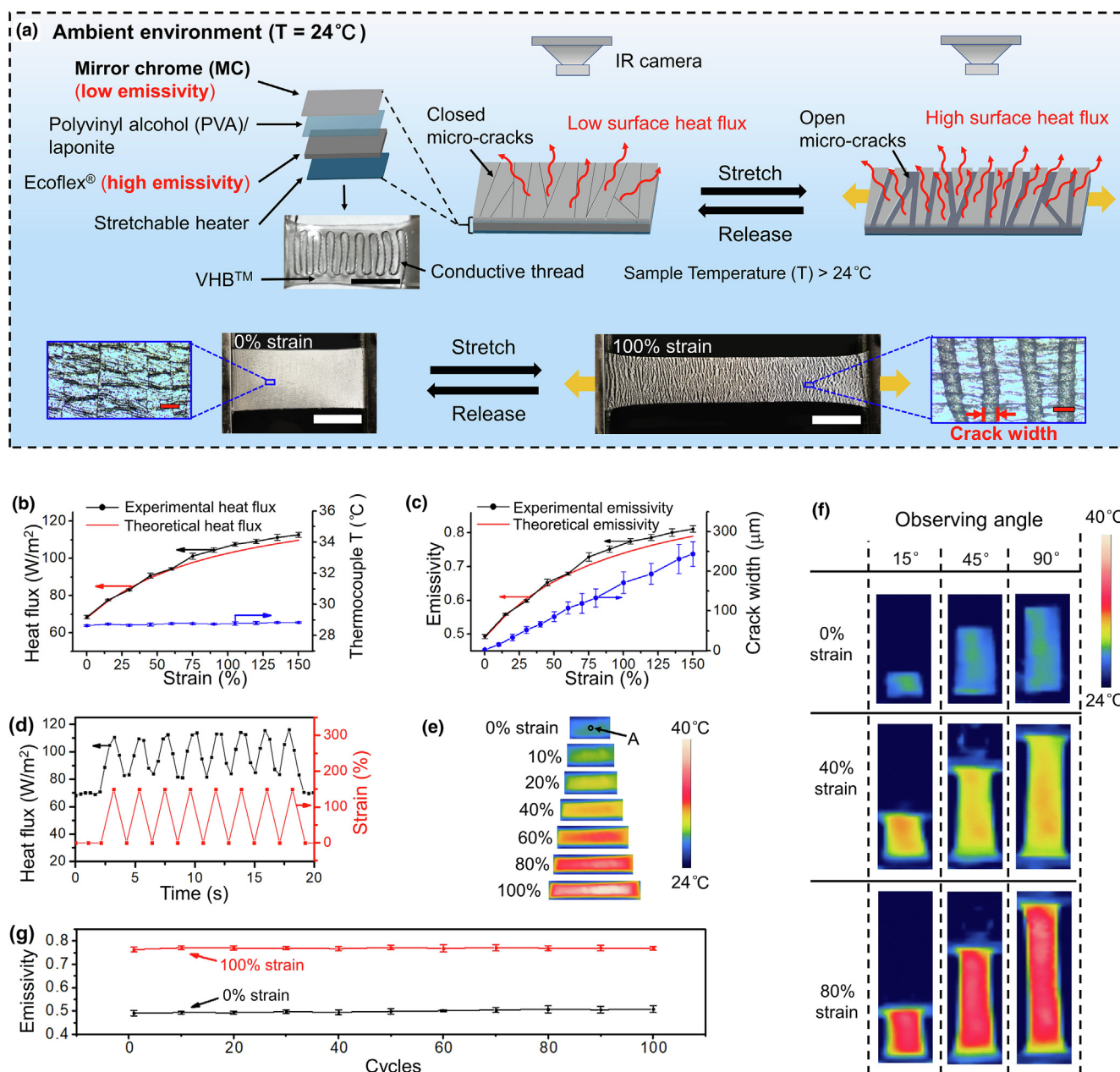


FIGURE 1

Schematic and characterizations of the TMSU. (a) Schematic of the TMSU structure and distributed cracked topography (black scale bar = 1 cm, white scale bar = 1 cm, red scale bar = 200 μm). (b) Strain response of the experimental and theoretical heat flux and thermocouple temperature of the TMSU. (c) Experimental and theoretical emissivity and crack width of the TMSU (with MC and PVA/laponite coating) as a function of strain. (d) Evolution of the heat flux of the TMSU and corresponding strain level as a function of time under an ultra-fast stretching/releasing rate (50% strain/s). (e) Thermal camera images (TCIs) of the TMSU under different uniaxial strains. (f) TCIs of the TMSU with 0%, 40%, and 80% strain and under different observing angles. (g) Reversibility of the emissivity at 0% and 100% strain upon stretching/releasing for 100 cycles.

20%, 80%, and 150% strain, respectively (see Fig. S3 for the strain response of the crack width and the crack area ratio indicating the area ratio of open cracks and the whole surface). Note that the incorporation of the PVA/laponite layer (thickness = 297 nm) beneath the MC coating layer (thickness = 310 nm) is crucial to achieve this high sensitivity for strain-responsive emissivity, because it effectively reduced the number of cracks and thus increased the average crack width. This is due to the increase of overall film thickness and the lower Young's modulus (E) of the PVA/laponite layer (~ 8 GPa) (E of the MC layer ~ 69 GPa),

which remarkably altered the film fracture behavior [40,41]. Therefore, the addition of PVA/laponite dramatically increased the crack width at each strain, such as 66.4 μm at 40% strain as compared to 10.8 μm for the counterpart with MC coating layer only (see Fig. S4(a) and S4(b)). The larger crack width at 40% strain allowed all the detectable IR radiation (wavelength ranging from 1.5 to 15 μm) to travel through the micro-cracks and reach the thermal camera. Also, if only PVA/laponite is used as the thin film layer without MC for the TMSU, the stretching process will not be able to create conspicuous changes in the effective emis-

sivity as both the substrate and the PVA/laponite layer have similar emissivities, larger than 0.9 (see Fig. S4(c)). Therefore, as shown in Fig. S4(d), the experimental emissivity of the TMSU with a PVA/laponite layer and MC thin film layer exhibited improved strain response with a 55.6% increase in emissivity at 100% strain, which is 2.2 folds higher than the counterpart with MC only, and notably the TMSU with PVA/laponite layer only as thin film showed virtually no change in emissivity as stretched.

Fig. 1(d) also shows that the heat flux of the TMSU can demonstrate instantaneous, reversible, and synchronized response under multiple ultra-fast stretching/releasing cycles without recognizable hysteresis (stretching rate = 50% strain/s, 13.5 mm/s). The strain response time of the evident heat flux change was tested as 0.4 s, which is already the maximum temporal resolution of the measuring sensor (thus, the real strain response time of the device is possibly even faster). As shown in Fig. S5(a), when the TMSU undergoes different stretching rates of 9.2% strain/s (2.5 mm/s), 6.3% strain/s (1.7 mm/s), and 4.4% strain/s (1.2 mm/s) from 0% to 150% strain, the heat flux manifests a faster change under a higher stretching rate but also exhibits virtually the same final values at 150% strain.

The temperature of an object recorded in a thermal camera is defined as the radiation temperature (T_{rad}), which is significantly affected by the emissivity of the object, and is not identical to the actual temperature (T) unless the object is a perfect emitter ($\epsilon = 1$) (see the Methods for details). Thus, the modulation of emissivity can be visualized as the change of T_{rad} captured in the thermography of thermal camera. As shown in Fig. 1(e), the thermal camera image (TCI) for the TMSU was displayed in pseudo-color with a spectrum palette mode, and the heated sample changed from blue-green at 0% strain ($T_{\text{rad}} = 24.7$ °C), to yellow at 20% strain ($T_{\text{rad}} = 26.8$ °C), red at 60% strain ($T_{\text{rad}} = 30.1$ °C), and red-white ($T_{\text{rad}} = 34.4$ °C) at 100% strain at the central position denoted as "A" (see Movie S1), and this highly sensitive "mechanochromic" response was also quantitatively interpreted by using the CIE color coordinates (see Fig. S5(b)). Thus, our system exhibits a 9.7 °C T_{rad} modulation change as stretched between 0% and 100% strain. Because the thermal radiation emitted from the TMSU has an omnidirectional characteristic, it enables the corresponding TCI to have remarkable observation angle independence. As shown in Fig. 1(f), the TCI of the heated sample exhibits the same color over a wide observing angle range from 15° to 90° at any strain (0%, 40%, and 80% strain as three representative examples shown in Fig. 1(f)). This intriguing angle independence invites opportunities for exploring unconventional properties and applications. Additionally, Fig. 1(g) demonstrates an excellent reversibility of the experimental emissivity of the TMSU under multiple stretching/releasing cycles between 0% and 100% strain, thanks to the strong interface between the PVA/laponite film and the Ecoflex® substrate formed by the covalent bonding [42].

TMSU applied for finger motion sensing and information encryption

As shown in Fig. 2(a), a modified TMSU without a stretchable heater was applied for finger motion sensing (up to 30% strain). The design is achieved by attaching the TMSU atop the bendable joint and unbendable part of a finger, with the finger serving

directly as the heater. The TCIs for sensing finger bending are shown in Fig. 2(b). As presented by the spectrum palette mode, the TMSU atop the unbendable part of the finger maintained a consistent blue color under different bending degrees. While the TMSU atop the bending joint demonstrated pseudo-color of blue at 0° of bending, green at 9°, green-yellow at 42°, and orange-yellow at 92°, whose color value is also quantitatively presented in the CIE color coordinates shown in Fig. S6 (also see Movie S2). The TCIs are also presented by a blue-grey duotone palette mode in Fig. 2(b), and the TMSU on the bendable middle part switches from blue to grey as the bending degree goes higher than 61°.

As shown in Fig. 2(c), the TMSU can also be applied as a strain responsive thermographic encryption device. In step 1, the PVA/laponite and Ecoflex® hybrid structure was pre-stretched to 100% strain and a "UCONN" patterned positive stencil mask was placed on top of the stretched sample. One MC layer was then spray coated on the sample surface followed by the removal of the mask (step 2). The sample was then totally released in step 3, followed by spray coating of another layer of MC over the entire sample surface (step 4). Thus, the original mask covered area (OMCA) only had one MC layer coated in the released state (0% strain), while the rest of the area (RA), not covered by the mask, had two MC layers coated at both 100% and 0% strain. Hence, the OMCA exhibits a topography with large open cracks that exposes the Ecoflex® substrate as stretched within 100% strain, while the substrate underneath the RA remains well shielded as stretched within same strain range, since no open cracks are observable in this area (see Fig. S7). Note that wrinkles form on the RA at strains <100% but will not affect the shielding effect (Fig. 2(c)). As shown in Fig. 2(d), the TCI of the heated sample was originally in a blue green color. Upon stretching to 100% strain, the "UCONN" pattern in orange red color was visible in the OMCA (also see Movie S3). As shown in Fig. 2(e), the heat flux and thermocouple temperature of the OMCA and RA were tested under stretching from 0% to 100% strain at a stretching rate of 9.2% strain/s. It is evident that the heat flux increased progressively with the strain from 67.2 to 106.3 W/m² in the OMCA. While the heat flux in RA remained virtually unchanged with some tiny fluctuation. The thermocouple temperatures in both the OMCA and RA were very close and barely changed during this dynamic stretching process. As such, this uniquely designed TMSU demonstrates that covert thermographic patterns can be simply and reversibly revealed by applied strain, which can potentially lead to the further development of next generation thermographic based encryption devices.

Design and performance of the thermal modulating system for bulging strain (TMSB)

We further design a thermal modulating system for bulging strain (TMSB) which experiences out-of-plane strain as driven by pneumatic actuation, where the MC, PVA/laponite, and Ecoflex® layers act as a deformable diaphragm in a circular shape with a substrate containing a heater and an inserted silicone tube for air inflation/deflation (see Fig. 3(a) and also Fig. S8 for the heater configuration). Pre-stretching treatment was also conducted to generate more distributed micro-cracks on the thin film layer (see Methods part). We denote the distance of the cen-

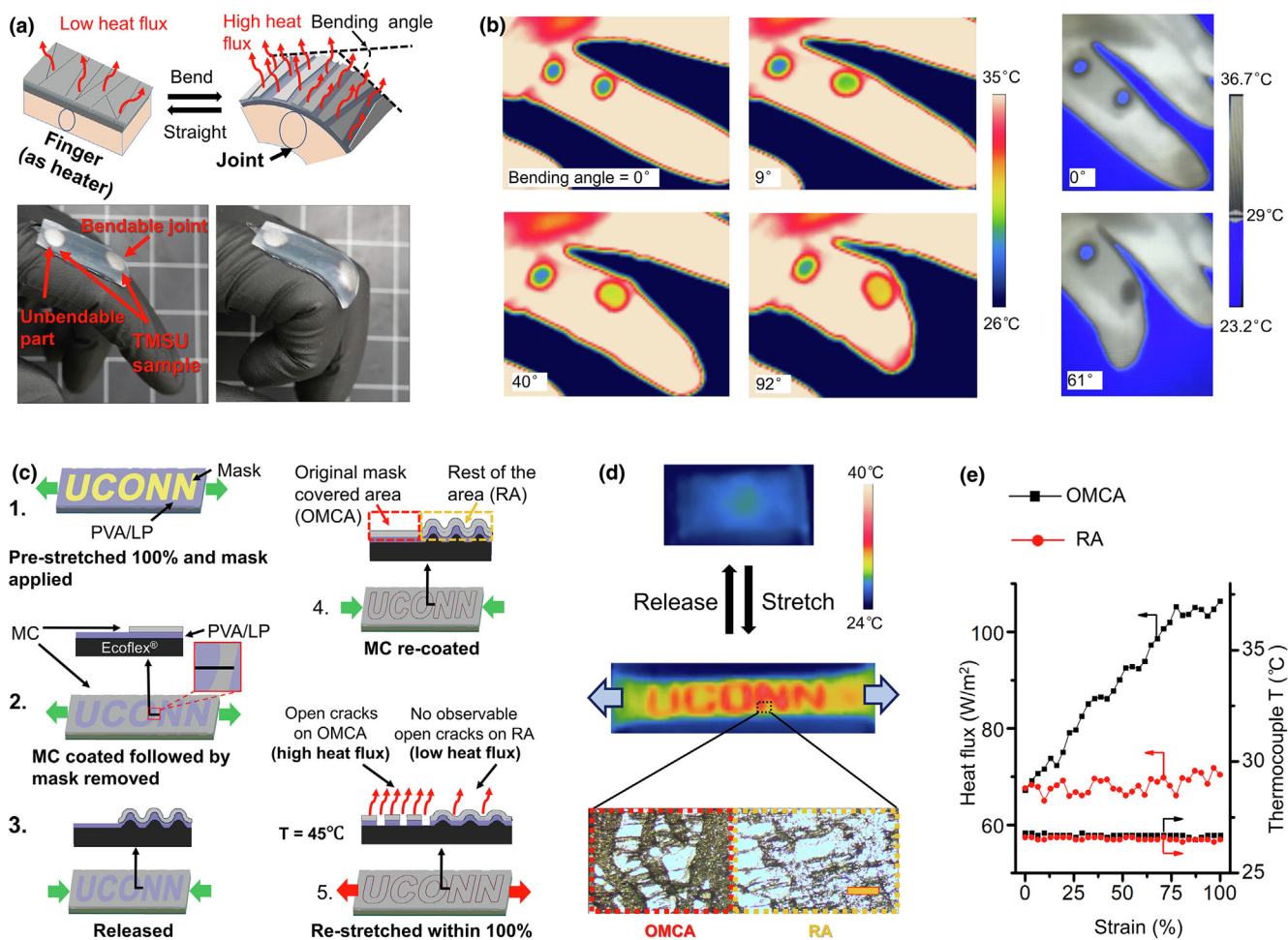


FIGURE 2

Application of the TMSU for finger motion sensing and information encryption. (a) Schematic and digital photos of the TMSU for finger motion sensing. (b) TCIs of the TMSU for finger motion sensing (in both spectrum palette mode and blue-grey duotone palette mode). (c) Schematic of the TMSU for information encryption device. (d) TCIs of the TMSU for encryption performance; the OM image shows the transition from OMCA to RA on the bottom part of the “N” letter as the sample stretched (scale bar = 200 μm). (e) Dynamic evolution of heat flux and thermocouple temperature as a function of strain for the TMSU (stretching rate = 9.2% strain/s).

ter of the bottom to the top of the spherical cap of the TMSB as deflection (d). The relationship of the deflection to the strain on the corresponding curved surface of the spherical cap and to the volume of the corresponding spherical cap are shown in Fig. S9 (a) and S9(b), respectively, which follows the well-established spherical cap model for bulge tests [43]. As evident in Fig. 3(b), the top thin film has distributed closed cracks at a released state. Upon inflation, the TMSB experiences bulging strain and expands into a spherical cap shape with the open cracks and the exposed substrate. The theoretical heat flux can be calculated by (see Methods for detail)

$$\bar{q} = \frac{(\varepsilon_e a^2 + \varepsilon_m d^2)}{a^2 + d^2} \sigma (T_s^4 - T_a^4) = \varepsilon_{\text{eff}} \sigma (T_s^4 - T_a^4) \quad (3)$$

where a is the initial radius of the plane circle, and the theoretical effective emissivity is given by $\varepsilon_{\text{eff}} = \frac{(\varepsilon_e a^2 + \varepsilon_m d^2)}{a^2 + d^2}$.

The experimental heat flux emitted from the TMSB was measured from 0% to 100% strain as shown in Fig. 3(c). It is evident that the heat flux increased progressively with the strain from

71.3 W/m² at 0% strain to 108.4 W/m² at 100% strain, which is consistent with the theoretical result. The corresponding thermocouple temperature of the testing area remained stable at ca. 28.2 °C. The strain response of the experimental and theoretical emissivity calculated from the heat flux data and the crack area ratio based on the optical microscopy (OM) image are shown in Fig. 3(d). The emissivity increased from 0.51 at 0% strain to 0.66, 0.71, and 0.78 at a strain of 40%, 80%, and 100%, respectively, which matched well with the theoretical calculation. The crack area ratio also increased from 0.18 at 20% strain to 0.52 at 80% strain. The TMSB also holds similar excellent reversibility under multiple inflation/deflation cycles to the TMSU (see Fig. S10(a)). The heat flux evolution from 0% to 100% strain as the TMSB underwent different dynamical inflation rates is shown in Fig. S10(b), exhibiting different growth trends but with virtually the same final values at 100% strain. The strain-dependent emissivity of the TMSB was also decoded by TCI under the spectrum palette mode (see Fig. 3(e)). The central part of the sample changed from blue ($T_{\text{rad}} = 26.6$ °C) at 0% strain, to yellow-orange ($T_{\text{rad}} = 28.1$ °C) at 40% strain, red

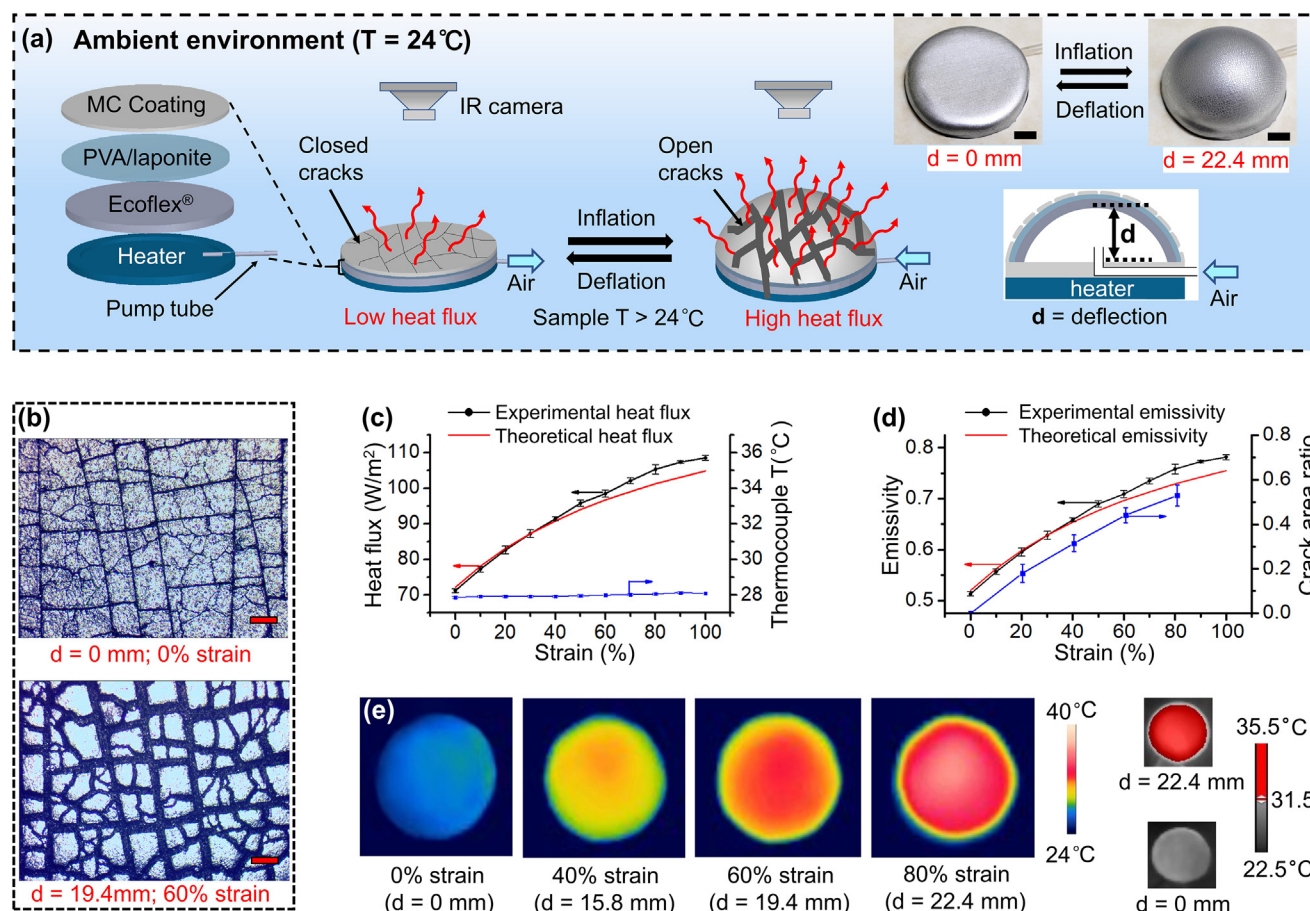


FIGURE 3

Schematic and characterizations of the TMSB. (a) Schematic of the TMSB (black scale bar = 1 cm). (b) OM images of the TMSB top surface at a deflection of 0 mm (0% strain) and 19.4 mm (60% strain). (c) Evolution of the experimental and theoretical heat flux and thermocouple temperature of the TMSB as a function of strain. (d) Experimental and theoretical emissivity and crack area ratio of the TMSB as a function of strain. (e) TCIs of the TMSB under different deflections.

($T_{\text{rad}} = 30.2\text{ }^{\circ}\text{C}$) at 60% strain, and red-white ($T_{\text{rad}} = 33.5\text{ }^{\circ}\text{C}$) at 80% strain (also see Fig. S10(c) for the quantitative interpretation in the CIE color coordinates). The TCI is also presented under the red-grey duotone mode, and a deflection of 22.4 mm (80% strain) can render the pseudo color of the sample to change from grey to red ($T_{\text{rad}} > 31.5\text{ }^{\circ}\text{C}$).

TMSB applied for multiplexing display and thermal camouflage

This pneumatically controlled TMSB with dynamic responses and multiplexing capability can be employed in an on-demand thermographic display. As shown in Fig. 4(a), a 3×3 array of the heated TMSB was placed on a frame. Upon selectively inflating different units with five cycles of operation, the five letters “uconn” were dynamically and rapidly displayed in a chronological order (also see Movie S4).

Since the TMSB can be arbitrarily moved and pneumatically controlled to tune its surface emissivity, it can autonomously conceal or reveal itself under the thermal camera. As shown in Fig. 4(b) and Movie S5, the heated TMSB (real $T = 45\text{ }^{\circ}\text{C}$) displayed blue pseudo-color was initially placed in a relatively cool area ($T_{\text{rad}} = 32.2\text{ }^{\circ}\text{C}$) manifested yellow color. Upon inflation to 14.1 mm (31.8% strain), the increased emissivity of the TMSB

allowed it to demonstrate the same T_{rad} as the cool area, which made it totally invisible under TCI. The TMSB was then moved to the hot area ($T_{\text{rad}} = 36.4\text{ }^{\circ}\text{C}$), in which its yellow pseudo-color can be spotted in the hot area in red. To conceal the TMSB again, further inflation was applied to rise the T_{rad} of the TMSB with a deflection of 20.1 mm (64.9% strain). The TMSB was then moved back to the cool area again, followed by a deflation to hide it again in the camera. Finally, further deflation was conducted to reveal the TMSB in the cool area. Fig. 4(c) shows the corresponding heat flux emitted from the TMSB as a function of time for the aforementioned process. It shows a gradual increase from $71.3\text{ W}/\text{m}^2$ at 0 s (step 1 shown in Fig. 4(b)) to $97.1\text{ W}/\text{m}^2$ at 15 s (step 6) followed by slowly decreasing back to $71.5\text{ W}/\text{m}^2$ at 27 s (step 9), which is consistent with the pseudo-color change shown in the TCI. As shown above, the TMSB demonstrates an extraordinary capability as an adaptive and autonomous soft thermal camouflage device.

In summary, we have designed a new cephalopod-inspired thermal radiation modulator based on a film-substrate hybrid structure, capable of dynamically controlling their surface thermal radiation through mechanical means with on-demand responses. The thermal modulation is achieved by mechanically

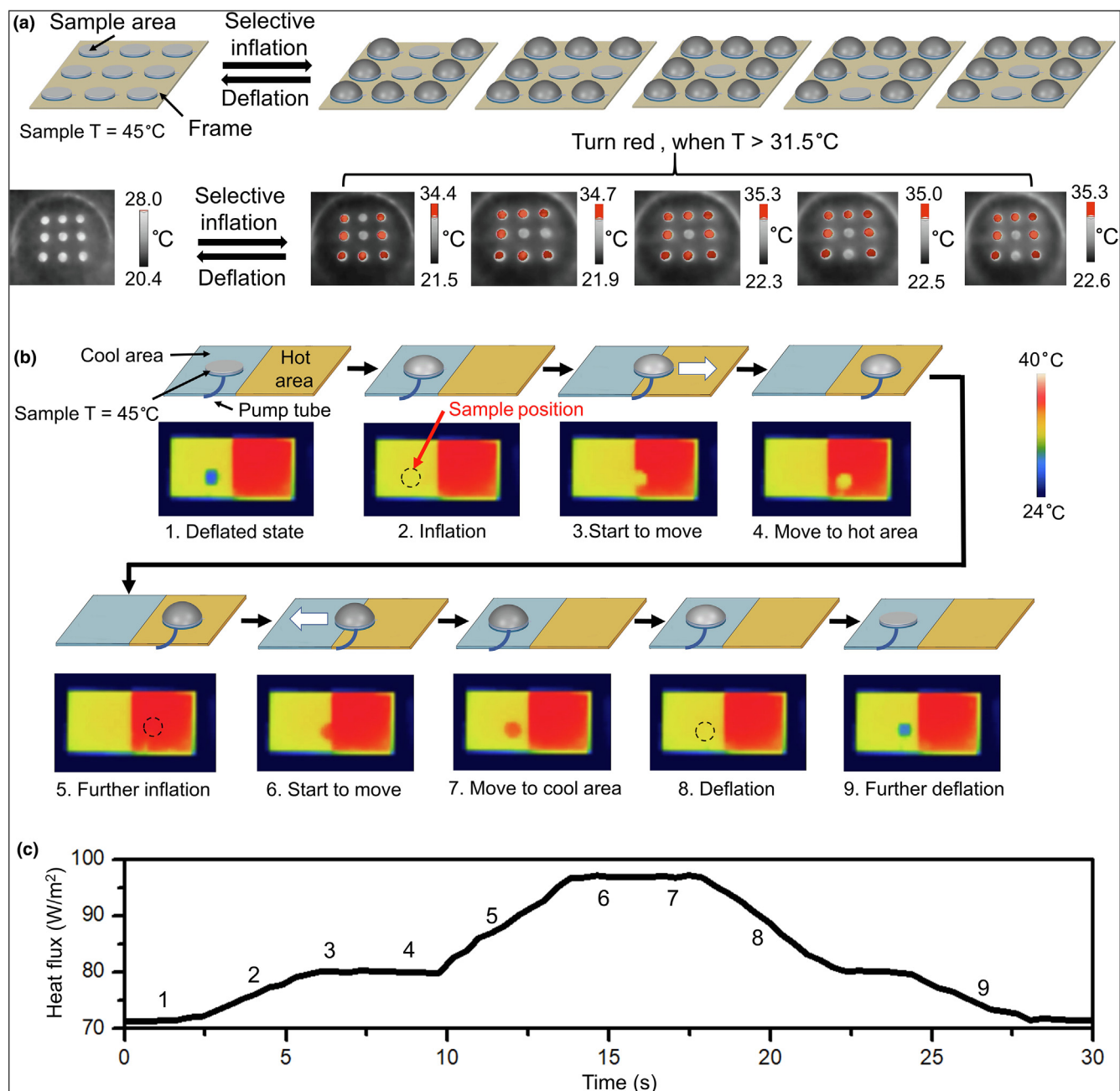


FIGURE 4

Design and performance of the TMSB based devices for dynamic display and thermal camouflage applications. (a) Schematic and performance in TCI of the TMSB arrays for multiplex dynamic display. (b) Schematic and performance in TCI of the TMSB device for thermal camouflage application. (c) Heat flux variation of the TMSB as a function of time for the steps shown in (b).

tuning the opening of the distributed micro-cracks in thin film layer with a low emissivity, and thus realizing the controllable exposure of the underlying soft substrate with a high emissivity. The system was modified into two types of structures for operating under uniaxial strain (i.e., TMSU) and bulging strain (i.e., TMSB). The strain-responsive heat flux and emissivity of this system was quantitatively measured and verified by the theoretical analysis from the Stefan-Boltzmann law. The emissivity of the TMSU can be varied between 0.49 and 0.81 within a uniaxial strain between 0% and 150%, which inspired the invention of an autonomous wearable finger motion sensor under thermo-

graphic vision and a mechanical responsive information encryption device. The TMSB driven by pneumatic actuation demonstrates emissivity changes from 0.51 to 0.78 between 0% and 100% strain, and it can be employed in a 3 × 3 thermographic display array and dynamic thermal camouflage with changing environmental temperature. This system presents a number of advantages, including ease of fabrication, low working temperature, high tunability, angle independence, robust structure with remarkable cyclability, instantaneous and on-demand response, high strain sensitivity, feasibility for patterning and multi-array, and ease for autonomous actuation. There-

fore, this work is expected to facilitate the creation of the next-generation thermal modulation devices with autonomous, on-demand, and wide range control, which can bring forth new opportunities to advance materials technologies and innovate functional devices with a broad spectrum of applications.

Methods and materials

Materials

The mirror chrome (MC) coating with a low emissivity (mainly containing aluminum flakes) was obtained from Spaz Stix, Inc. The PVA/laponite composite was comprised of PVA (Kuraray POVAL™ 28–99, M_w (weight average molecular weight) $\sim 145,000$, $\sim 99\%$ degree of hydrolysis) and laponite (BYK Additives Inc., mass ratio of PVA:laponite = 3:2). Ecoflex® 00-30 was used as the substrate material (containing Part A and Part B precursors with a weight ratio = 1:1, Smooth-On, Inc.). The conductive thread (diameter: ca. 0.12 mm) was purchased from Sparkfun Electronics. Silicone adhesive was purchased from Loctite, Inc. Allyl isocyanate is purchased from Sigma Aldrich.

Preparation of a thermal radiation modulating system for uniaxial strain (TMSU)

A layer of uniform PVA/laponite composite film with a thickness of ca. 297 nm was cast on a pre-cleaned polystyrene foundation (from Fisher Scientific™) using a 5 mg/mL PVA/laponite aqueous dispersion, followed by the treatment of allyl isocyanate. An Ecoflex® 00-30 precursor was cast atop the allyl isocyanate treated PVA film followed by curing at 80 °C for 2 h (thickness of the Ecoflex® layer ≈ 1.5 mm). This process enabled the PVA film to form covalent bonding with the Ecoflex® substrate. The bilayer material was then peeled off carefully from the foundation in one direction which create distributed cracks, followed by spray coating a layer of mirror chrome (MC) (ca. 310 nm in thickness) atop the PVA/laponite composite film by an airbrush style spray-gun (Master Airbrush G444-SET, equipped with a 0.5 mm needle nozzle and a Royal Mini Air Compressor, TC-20B). Note that the high uniformity of the PVA/laponite film with a strong film-substrate interface results in the formation of ordered crack distribution on the thin film layer during the peeling process. The multi-layered structure was then cut into a rectangle shape (2.7 cm \times 1.2 cm). To prepare the stretchable heater, conductive thread spun from stainless steel fibers was adhered to a VHB™ 4910 double-sided adhesive tape (2.7 cm \times 1.2 cm) with a serpentine pattern as shown in Fig. S1. Another 3 M VHB™ 4910 double-sided adhesive tape of the same dimensions was attached atop the conductive thread to make a sandwich-like structure. The stretchable heater was then attached to the bottom of the multi-layered structure by the silicone adhesive. The sample was fixed on a custom-built stretcher and pre-stretched to 200% strain to generate a more distributed micro-cracks prior to being released back to 0% strain.

Preparation of a modified TMSU for finger motion sensing

The preparation procedures for the PVA/laponite composite layer and Ecoflex® layer were the same as the aforementioned procedures. The bilayer was then cut into a size of 1.2 cm \times 3.0 cm after being peeled away from the foundation. A stencil mask with two circles (diameter = 7 mm) was placed atop the PVA/laponite

composite layer surface prior to the spray coating of the MC with a thickness of ca. 310 nm. Upon the removal of the stencil mask, the sample demonstrated two circle-shaped areas with MC coating as shown in Fig. 2(a). The sample was then fixed on a custom-built stretcher and pre-stretched to 200% strain to generate distributed cracks, followed by releasing back to 0% strain. Subsequently, the sample was attached on the top of a finger part of a nitrile butadiene rubber glove, with one circle with MC coating being right atop a bendable part/joint of the finger, while the other one being right atop an unbendable part of the finger.

Preparation of a modified TMSU for encryption application

The preparation procedures for the PVA/laponite composite layer and Ecoflex® substrate was the same as the aforementioned procedures. The bilayer was then cut into a size of 2.0 cm \times 4.0 cm after being peeled away from the foundation and then attached to the top of a stretchable heater (2.0 cm \times 4.0 cm) by the silicone adhesive. As shown in Fig. 2(c), after the sample was pre-stretched to 100% strain, a “UCONN” patterned stencil mask was placed atop the PVA/laponite composite layer followed by spray coating a MC layer (thickness ≈ 210 nm). Upon the removal of the stencil mask and the release of the sample, the mask covered area remained uncoated by MC. After the sample was released to 0% strain, another layer of MC (thickness ≈ 150 nm) was spray coated on the entire sample surface. The sample was then fixed on a custom-built stretcher and pre-stretched to 200% strain to generate distributed micro-cracks, followed by being released back to 0% strain.

Preparation of a thermal radiation modulating system for bulging strain (TMSB) for dynamic display and thermal camouflage

The preparation procedures for the PVA/laponite composite layer and Ecoflex® substrate was the same as the aforementioned procedure. The bilayer was then cut into a circular shape with a diameter of 5.0 cm after being peeled away from the foundation. A layer of MC (thickness ≈ 310 nm) was then spray coated atop the PVA/laponite composite layer. Since the peeling process will introduce micro-cracks perpendicular to the peeling direction on the MC and the rigid PVA/laponite composite thin film, a 100% bi-axial pre-stretching strain was applied (one stretching direction is aligned with the original cracks orientation), followed by releasing back to 0% strain. The heater was prepared by attaching a conductive thread in a serpentine pattern atop a circular shaped VHB tape with a polystyrene disk at the bottom (diameter = 5.0 cm) as shown in Fig. S8. The multi-layered structure, the heater, and a silicone tube connected to a syringe for inflation/deflation were then stacked and attached together in the fashion as shown in Fig. 3(a) by the silicone adhesive. In order to generate additional distributed micro-cracks via bulging strain, the as-prepared TMSB was inflated to a deflection of 25 mm (100% strain) followed by being released.

Theoretical calculation of the heat flux and the emissivity of the TMSU and TMSB

Results for the TMSU. For the convenience of analyzing the TMSU, we assume that the initial released state of the sample follows a pattern as shown in the Fig. S2. The closed cracks (the red lines)

are distributed periodically on the surface with a distance l_0 , and the region between them are covered with the MC and PVA/laponite layers. Since the stretch deformation is nearly uniform, we take a unit cell (the region in the dash square where the crack is located in the middle) to compute the change of the emissivity in response to the stretch.

According to the Stefan-Boltzmann law, the total heat flux from a gray body is given by

$$q = A\varepsilon\sigma(T_s^4 - T_a^4) \quad (\text{a})$$

where $\sigma = 5.6703 \times 10^{-8} \text{ (W/m}^2\text{K}^4\text{)}$ is the Stefan-Boltzmann constant, T_s and T_a are temperatures of the sample and the ambient environment, respectively, A is the surface area of the sample and ε is the emissivity. In our experiment, the sample temperature remains unchanged during the elongation process, and thus the variation of average heat flux per unit area, $\bar{q} = q/A$, is mainly induced by the change of area A and the emissivity constant ε . According to the experimental results, we observed that the width of the sample, h_0 , doesn't significantly change before and after stretch, so the area increase of the stretched sample is mainly induced by its elongation. Meanwhile, the thin film layer is much stiffer (the Young's modulus for MC: $\sim 69 \text{ GPa}$ and the Young's modulus for PVA/laponite: $\sim 8 \text{ GPa}$) than the bottom Ecoflex[®] substrate (the elastic modulus: $\sim 68 \text{ kPa}$), and thus the stretch of the sample is mainly supplied by increasing the crack width, ascribing to the elongation and exposure of the underneath Ecoflex[®] substrate. Accordingly, the surface area of the stretched unit cell is given by

$$A = (\lambda l_0 + l_0)h_0 = A_m + A_e \quad (\text{b})$$

where λ is the total stretch strain of the sample, l_0 and λl_0 are the length of the thin film layer and the total length of cracks (Fig. S2), respectively. Here, $A_m = l_0 h_0$ and $A_e = \lambda l_0 h_0$ represent the surface area of the MC top surface and the exposed Ecoflex[®] substrate, respectively.

In a stretched sample, the total heat flux comes from the regions occupied by the MC layer and the exposed Ecoflex[®] substrate. Hence, according to Eqs. (a) and (b), the average heat flux per unit area is calculated by

$$\bar{q} = \frac{\sigma(T_s^4 - T_a^4)(\varepsilon_m A_m + \varepsilon_e A_e)}{A_m + A_e} = \varepsilon_{\text{eff}}\sigma(T_s^4 - T_a^4) \quad (\text{c})$$

where ε_m and ε_e are the emissivity coefficients of the MC layer and Ecoflex[®] substrate, respectively and ε_{eff} is an effective emissivity coefficient of the sample.

$$\varepsilon_{\text{eff}} = \frac{\varepsilon_m + \lambda\varepsilon_e}{1 + \lambda} \quad (\text{d})$$

In the initial state with $\lambda = 0$, we obtain from Eq. (d) that $\varepsilon_{\text{eff}} = \varepsilon_m$, while in the fully stretched state for an extremely large λ , ε_{eff} approximates to ε_e .

Results for the TMSB. To calculate the heat flux and emissivity of the TMSB (Fig. 3a), the total area of the inflated bulge satisfies $\pi(a^2 + d^2)$, where a is the initial radius of the plane circle and d is the height of the bulge (the distance of the center of the bottom to the top of spherical cap). The MC and PVA/laponite thin film layer after inflation is nearly equal to the initial state due to its high stiffness compared to the Ecoflex[®], and thus the surface

area of the MC is equal to its initial area and can be given by, $A_m = \pi a^2$. The area occupied by the open crack with the exposure of Ecoflex[®] layer is thus given by $A_e = \pi(a^2 + d^2) - \pi a^2 = \pi d^2$. Using a similar calculation approach to Eq. (c), the average heat flux is calculated by

$$\bar{q} = \frac{(\varepsilon_e d^2 + \varepsilon_m a^2)}{a^2 + d^2} \sigma(T_s^4 - T_a^4) = \varepsilon_{\text{eff}}\sigma(T_s^4 - T_a^4) \quad (\text{e})$$

where the effective emissivity is given by $\varepsilon_{\text{eff}} = \frac{(\varepsilon_e d^2 + \varepsilon_m a^2)}{a^2 + d^2}$. We can verify that $\varepsilon_{\text{eff}} = \varepsilon_m$ in the initial flat state with $d = 0$ and ε_{eff} approaches ε_e for a fully inflated state with a large displacement d .

Characterizations

The thermal camera images and videos were captured by a FLIR E5-XT Infrared camera. The temperature of an object recorded in the thermography of this camera is defined as radiation temperature (T_{rad}), which is not identical to the real temperature (T) unless the object is classified as black body. The determination of T_{rad} can be defined as follows: $T_{\text{rad}} = C \times P_o(T) = C \int_{\lambda_1}^{\lambda_2} \varepsilon_o(\lambda) \times \frac{2\pi h c^2}{\lambda^5} \frac{1}{e^{hc/\lambda k_B T} - 1} d\lambda$ where, C is the constant of a thermal camera, P_o is the emission power from the object collected by a thermal camera, and ε_o is the emissivity of the object. $[\lambda_1, \lambda_2]$ is the spectral measuring range of the thermal camera, which is from 1.5 to 15 μm for the camera in this work. The heat flux and thermocouple temperature were tested by a FluxDAQ heat flux and thermocouple measurement system. To measure the real temperature of the sample, a thermocouple temperature sensor was placed in contact with the sample surface. The FluxDAQ measurement system was used to convert the thermocouple signals to temperature data. The emissivity of the sample was obtained from measuring the corresponding heat flux based on the classical Stefan-Boltzmann law, which can be derived from Eq. (1): $\varepsilon_s = \bar{q}/\sigma(T_s^4 - T_a^4)$, where ε_s is the emissivity of the sample, \bar{q} is the average heat flux per unit area emitted from the sample to the ambient environment, σ is a constant and equal to $5.6703 \times 10^{-8} \text{ (W/m}^2\text{K}^4\text{)}$, T_s and T_a are the temperatures of the sample and ambient environment, respectively (T_a was 24 °C in the test). Therefore, to measure the emissivity, the sample was heated to a stable preset temperature (such as 45 °C) as confirmed by the thermocouple. Subsequently, the heat flux sensor was placed atop the sample surface with a distance of 5 mm to record the stable heat flux value that can be used to calculate the emissivity. The optical microscopic images of all of the samples were recorded on an AmScope ME 520TA optical microscope in reflective mode. All of the digital photos and videos were captured by a Sony rx100m6 camera. The CIE color coordinates for the samples were created via analyzing the thermal camera image by the Adobe Photoshop CS4 software.

CRedit authorship contribution statement

Songshan Zeng: Conceptualization, Methodology, Investigation, Data curation, Writing - original draft, Writing - review & editing, Visualization. **Kuangyu Shen:** Methodology, Investigation, Data curation, Writing - original draft, Writing - review & editing, Visualization. **Yin Liu:** Formal analysis, Data cura-

tion, Writing - original draft, Writing - review & editing. **Aimee P. Chooi:** Investigation, Data curation, Writing - review & editing, Visualization. **Andrew T. Smith:** Data curation, Writing - review & editing. **Shihao Zhai:** Methodology, Investigation. **Zi Chen:** Formal analysis, Data curation, Writing - review & editing, Supervision. **Luyi Sun:** Conceptualization, Methodology, Writing - review & editing, Supervision, Project administration.

Declaration of Competing Interest

The authors declare that they have no known competing financial interests or personal relationships that could have appeared to influence the work reported in this paper.

Acknowledgements

We acknowledge Kuraray for providing the polyvinyl alcohol sample. A.T.S. acknowledges the GAANN Fellowship (No. P200A150330). The authors thank Zaili Hou, Peng Fan, Wyatt Bush, and Dajian Huang for their helpful suggestions and assistance in experiments.

Data availability

The original data for this study are available from the corresponding authors upon request.

Appendix A. Supplementary data

Supplementary data to this article can be found online at <https://doi.org/10.1016/j.mattod.2020.12.001>.

References

- [1] R. Hanlon, *Curr. Biol.* 17 (11) (2007) R400.
- [2] Hanlon, R. T., et al., *Philos. Trans. R. Soc. Lond. B Biol. Sci.* 364 (1516), (2009) 429..
- [3] S. Zeng et al., *Nat. Commun.* 7 (1) (2016) 11802.
- [4] S. Zeng et al., *Mater. Horiz.* 7 (1) (2020) 164.
- [5] Y. Li et al., *Nat. Commun.* 9 (1) (2018) 273.
- [6] E.M. Leung et al., *Nat. Commun.* 10 (1) (2019) 1947.
- [7] Q. Wang et al., *Nat. Commun.* 5 (1) (2014) 4899.
- [8] J. Teyssier et al., *Nat. Commun.* 6 (1) (2015) 6368.
- [9] L. Phan et al., *Chem. Mater.* 28 (19) (2016) 6804.
- [10] L.M. Mäthger, R.T. Hanlon, *Cell Tissue Res.* 329 (1) (2007) 179.
- [11] Y. Sun et al., *ACS Appl. Mater. Interfaces* 11 (14) (2019) 13538.
- [12] O. Salihoglu et al., *Nano Lett.* 18 (7) (2018) 4541.
- [13] S.P. Singh et al., *Packag. Technol. Sci.* 21 (1) (2008) 25.
- [14] A.P. Raman et al., *Nature* 515 (7528) (2014) 540.
- [15] P.C. Hsu et al., *Science* 353 (6303) (2016) 1019.
- [16] A. Lenert et al., *Nat. Nanotechnol.* 9 (2) (2014) 126.
- [17] O. Ilic et al., *Nat. Nanotechnol.* 11 (4) (2016) 320.
- [18] A. Mech et al., *J. Am. Chem. Soc.* 132 (13) (2010) 4574.
- [19] T. Asano et al., *Sci. Adv.* 2 (12) (2016) e1600499.
- [20] L. Xiao et al., *Nano Lett.* 15 (12) (2015) 8365.
- [21] H. Ji et al., *RSC Adv.* 7 (9) (2017) 5189.
- [22] S. Vasant et al., *Appl. Phys. Lett.* 102 (8) (2013) 081125.
- [23] Y. Huang et al., *Appl. Phys. Lett.* 105 (24) (2014) 244102.
- [24] R. Brooke et al., *J. Mater. Chem. C* 5 (23) (2017) 5824.
- [25] M.G. Hutchins et al., *Electrochim. Acta* 46 (13) (2001) 1983.
- [26] Z.J. Coppens, J.G. Valentine, *Adv. Mater.* 29 (39) (2017) 1701275.
- [27] Z. Cheng et al., *ACS Appl. Mater. Interfaces* 7 (49) (2015) 27494.
- [28] Y. Qu et al., *Light Sci. Appl.* 7 (1) (2018) 26.
- [29] S. Chandra et al., *ACS Photonics* 5 (11) (2018) 4513.
- [30] T. Lim et al., *Appl. Mater. Today* 20 (2020) 100624.
- [31] Y. Wang et al., *Proc. Natl. Acad. Sci. U.S.A.* 116 (43) (2019) 21361.
- [32] M. Sala-Casanovas et al., *Nanoscale Microscale Thermophys.* 23 (3) (2019) 173.
- [33] Y. Ke et al., *Nano Energy* 73 (2020) 104785.
- [34] Y. Li et al., *Adv. Funct. Mater.* 30 (5) (2020) 1907451.
- [35] C. Xu et al., *Adv. Mater.* 32 (16) (2020) 1905717.
- [36] L. Tomholt et al., *Energy Build.* 226 (2020) 110377.
- [37] C. Xu et al., *Science* 359 (6383) (2018) 1495.
- [38] Y.M. Guo et al., *Int. J. Thermophys.* 40 (1) (2018) 10.
- [39] V. Shatikian et al., *Int. J. Heat Mass Transf.* 51 (5–6) (2008) 1488.
- [40] X.C. Zhang et al., *J. Appl. Phys.* 103 (2) (2008) 023519.
- [41] H.M. Yin et al., *Int. J. Fract.* 153 (1) (2008) 39.
- [42] S. Zeng et al., *Mater. Horiz.* 7 (9) (2020) 2368.
- [43] C. Yanfei et al., *J. Appl. Mech.* 84 (6) (2017) 061005.